

First-principles calculation of the electronic nematicity in FeSe

Xuanyu Long,¹ Shunhong Zhang,² Fa Wang,^{3,4} and Zheng Liu^{1,4,*}

¹*Institute for Advanced Study, Tsinghua University, Beijing 100084, China*

²*International Center for Quantum Design of Functional Materials (ICQD),*

Hefei National Laboratory for Physical Sciences at the Microscale,

*and Synergetic Innovation Center of Quantum Information and Quantum Physics,
University of Science and Technology of China, Hefei, Anhui 230026, China*

³*International Center for Quantum Materials, School of Physics, Peking University, Beijing 100871, China*

⁴*Collaborative Innovation Center of Quantum Matter, Beijing 100084, China*

(Dated: March 5, 2022)

We report a density functional theory calculation that produces the nonmagnetic electronic nematic state in FeSe, without explicit breaking of the tetragonal lattice symmetry. We incorporate orbital-resolved interactions by +U and hybrid functional, and precondition the initial wavefunction to find local energy minima with spontaneous symmetry breaking. The lowest-energy nematic state we find features an anti-ferro hexadecapolar charge order, instead of a simple ferro-orbital order, which is important to produce the correct Fermi surface topology in FeSe. We propose that the weak inversion symmetry breaking induced by this multipolar order can be detected by high-precision measurement of the band dispersion as well as second-harmonic generation.

First-principles calculation within the framework of density function theory (DFT) has played an important role in understanding the iron-based superconductors. For the high-temperature phase, the standard local density approximation can already qualitatively describe the Fermi surface topology and its orbital components [1–3]. For the magnetic phase, the local spin density approximation or its generalized gradient approximation (GGA) extension can obtain the correct ground-state spin order in most cases [1, 2, 4]. Additional corrections to the electronic correlation effects, e.g. the dynamical mean-field theory (DMFT), further reduce some quantitative discrepancies, such as the overestimation of the bandwidth and the magnetic moment [5, 6].

However, a first-principles description of the nematic order remains elusive. Dictated by a C_4 rotational symmetry breaking, the nematic phase typically resides between the high-temperature symmetric phase and the low-temperature magnetic phase [7]. The attempt to explicitly break the C_4 symmetry by straining the lattice in the DFT simulation results in only negligible changes on the electronic structure [8], which is not surprising, since there is strong experimental evidence suggesting that the nematic order is of an electronic origin [9].

There are two main scenarios to explain the electronic mechanism of nematicity [7]. One is to view it as a precursor of the magnetic phase, in which the spin quadrupolar fluctuation first diverges before the ordering of the spins [10–12]. The other is to invoke a spontaneous ferro-orbital ordering [13–15]. In general, these two types of order parameters are intertwined [16], and the C_4 symmetry breaking manifests in both the spin and the orbital degrees of freedom simultaneously.

From the DFT perspective, there is no apparent way to take a composite spin order into account. Nevertheless, orbital-resolved approaches, e.g. the +U [17] or hybrid

functional [18], renders probe of the nematic order in the orbital channel. We consider FeSe as an ideal target to perform such kind of calculation, because no magnetic order has thus far been observed in FeSe, unless high pressure is applied [19]. Considering that the magnetic correlation remains small within the nematic phase [20], it is reasonable to speculate that the orbital instability might be more noticeable. In addition, inspired by the high superconducting transition temperature of monolayer FeSe on SrTiO_3 substrate [21, 22], extensive experimental data have been collected and crosschecked, in particular high-resolution angle-resolved photoemission spectroscopy (ARPES) data [8, 23–38], and thus systematic evaluation of the calculation results is possible.

The main finding of this Letter is that for FeSe a non-magnetic state with C_4 symmetry breaking can indeed be self-consistently obtained from first principles. More surprisingly, the calculation also suggests unexpected multipole order, which further reconstructs the Fermi surface, and reproduces important features of the electronic structure as observed experimentally. In previous theories, orbital splitting with opposite signs around Γ and M points is the dominant order parameter which reproduces the ARPES observations [39–41], but this order parameter cannot arise from mean-field treatment of local correlations on single Fe atoms, and sophisticated many-body theory has to be employed to generate it [40, 41]. Our results show that the ARPES Fermi surface topology can be reproduced by careful treatment of local correlations in DFT.

DFT can be viewed as a Landau-type field theory $E_{DFT}[\rho(\mathbf{r})]$, in which the electron density $\rho(\mathbf{r})$ acts as the order parameter dictating the energy of the system, and the first-principles calculation is to search for the ground state electron density $\rho_{GS}(\mathbf{r})$ that minimizes E_{DFT} . It is possible to enlarge the energy functional

into $E_{DFT}[\rho(\mathbf{r}), \mathbf{s}(\mathbf{r})]$ by including spin density $\mathbf{s}(\mathbf{r})$ as another order parameter. These two order parameters naturally cover the charge density wave and spin density wave instabilities. It is understood that if the ground-state many-body wavefunction $|\Psi_{GS}\rangle$ is known, the order parameters are calculated as $\rho_{GS}(\mathbf{r}) = \langle \Psi_{GS} | \hat{n}(\mathbf{r}) | \Psi_{GS} \rangle$ and $\mathbf{s}_{GS}(\mathbf{r}) = \langle \Psi_{GS} | \hat{\mathbf{S}}(\mathbf{r}) | \Psi_{GS} \rangle$, in which \hat{n} and $\hat{\mathbf{S}}$ are the particle number and spin operators, respectively.

One important numerical issue not sufficiently addressed before is that for a correlated system like FeSe, the landscape of E_{DFT} could be rather complicated, and thus the numerical minimization could be easily trapped to some local minimum point [42]. The common practice to perform the DFT minimization [43–45] is to iteratively update a set of auxiliary single-particle orbitals, so-called Kohn-Sham orbitals $\{\psi_i(\mathbf{r})\}$, which connects with electron density as $\rho(\mathbf{r}) = \sum_i f_i |\psi_i(\mathbf{r})|^2$ and f_i is the occupation function. Starting from an initial $\rho_0(\mathbf{r})$ that respects the full symmetry of the underlying lattice, the iteration can easily end at a $\rho_{GS}(\mathbf{r})$ without symmetry breaking, if a symmetric local minimum exists. Therefore, to probe potential symmetry breaking, it is beneficial to purposely drag $\rho_0(\mathbf{r})$ away from the symmetric basin by preconditioning the initial $\{\psi_i(\mathbf{r})\}$. For example, to test whether the nematic order can spontaneously develop, we first generate a set of $\psi_i(\mathbf{r})$ from a preparatory calculation on a manually distorted FeSe lattice that explicitly breaks the four-fold rotation symmetry. Then this set of $\{\psi_i(\mathbf{r})\}$ is fed to an undistorted FeSe lattice as a starting point to see whether it flows to a different local minimum. We note that preconditioning is merely a numerical treatment to better search the complicated energy landscape. It does not change the landscape. In other words, no matter how the initial $\{\psi_i(\mathbf{r})\}$ is preconditioned, the energy functional $E_{DFT}[\rho(\mathbf{r})]$ for the production run is always ensured to be an invariant of the space group P4/nmm. Besides preconditioning, the minimization algorithm is also a matter of concern. We notice that the damped velocity friction algorithm (for electronic minimization) sometimes has a better performance of escaping a shallow local minimum than the blocked Davidson iteration scheme and the direct inversion in the iterative subspace scheme [44].

Another important point we should note is that all the calculations below focus on the $\mathbf{s}(\mathbf{r}) = 0$ basin. This choice is based on the experimental fact that no intrinsic magnetic ordering transition has been observed in FeSe, and it is theoretically speculated that the ground state is a quantum paramagnet [46]. As long as $|\Psi_{GS}\rangle$ does not break the time-reversal symmetry, $\langle \Psi_{GS} | \hat{\mathbf{S}}(\mathbf{r}) | \Psi_{GS} \rangle$ is guaranteed to be zero. We note that spin fluctuation, i.e. a nonvanishing $\langle \Psi_{GS} | \hat{\mathbf{S}}^2(\mathbf{r}) | \Psi_{GS} \rangle$, will certainly renormalize the electronic structures as demonstrated by DMFT [5, 6]. In the present work, this effect is not explicitly taken into account.

The previous DFT works have shown that starting from an initial state with large spin polarization, the minimization can converge to various magnetic configurations with almost degenerate energy [47, 48]. However, none of these magnetic configurations naturally reproduces the ARPES band structure. Some DFT studies suggested artificially adopting higher-energy magnetic configurations, e.g. a Néel order [36, 49] or a superposition of multiple magnetic configurations [50] in order to improve the description. Technically, there is no wonder that $\mathbf{s}(\mathbf{r})$ can provide an additional knob to tune the electronic structure. However, in our calculation, we insist that the time-reversal symmetry should not be explicitly broken. For clarity, we remove $\mathbf{s}(\mathbf{r})$ from the functional in the following discussion.

With the considerations above, $E_{DFT}[\rho(\mathbf{r})]$ is constructed from the experimental lattice of bulk FeSe [51] and the minimization is performed starting from various initial $\{\psi_i(\mathbf{r})\}$. We first try Perdew-Burke-Ernzerhof functional [52] - one of the most widely employed GGA functional. *The calculation does not give any $\rho_{GS}(\mathbf{r})$ with symmetry breaking, which suggests that the standard DFT functional is insufficient to describe the nematic order.* This result is in some sense expected, since the nematic order is closely related to the strong interactions among the Fe 3d-orbitals, where the deficiency of the standard DFT is seen most clearly.

There are two widely-employed recipes to improve the description of localized orbitals. One is the DFT+U method [17], and the other is hybrid functional [18]. One unified view on these two recipes is that they both attempt to cancel the most conspicuous errors in the standard DFT functional - the Hartree potential of an electron with itself, which is significant for a localized orbital. Accordingly, the +U method re-evaluates the interaction terms by projecting $\rho(\mathbf{r})$ onto the local orbitals and explicitly exclude the self-interaction term. On the other hand, the hybrid functional incorporates a portion of the exact Fock energy that is also expected to cancel the unphysical self-interaction. Although both recipes still stay within the Hartree-Fock level, they were shown to give a qualitative improvement compared with the standard DFT, when applied to a wide range of transition metal and rare-earth metal compounds.

It is insightful to inspect how such a correction will modify the $E_{DFT}[\rho(\mathbf{r})]$ landscape based on the simplest rotational invariant DFT+U functional as introduced by Dudarev et al. [53]: $E_{DFT+U} = E_{DFT} + \frac{U}{2} \sum_j (Tr \tilde{n}_j - Tr \tilde{n}_j^2)$, in which j labels the Fe site, and \tilde{n}_j is the density matrix within the 3d-orbital subspace. Explicitly, $\tilde{n}_j^{\alpha\beta} = \sum_i f_i \langle j\alpha | \psi_i \rangle \langle \psi_i | j\beta \rangle$, in which α and β label the five 3d-orbitals of the j -th Fe atom. The first term $Tr \tilde{n}_j$ in the summation is the total occupancy of the 3d-orbitals, which is designed to adjust the total energy such that the correction term vanishes if the local orbitals are fully occupied or empty. We note that this term could

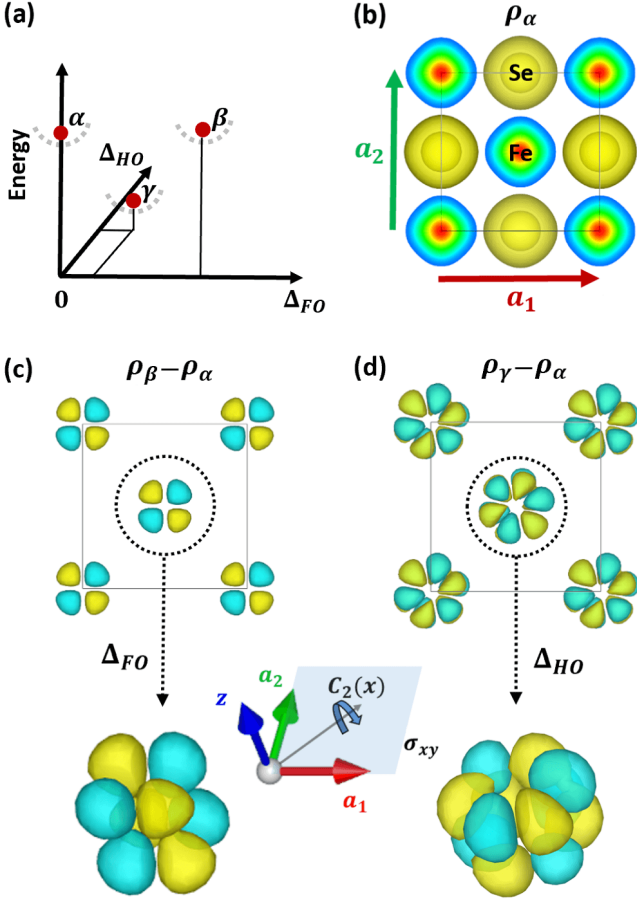


FIG. 1. (a) Schematic of the three local minimum points in the energy landscape. (b) Charge density contour at the symmetric local minimum (ρ_α) with $a_{1,2}$ as the two lattice vectors of the 2-Fe unit cell; (c) and (d) Charge density change at the two symmetry-breaking local minima ($\delta\rho_\beta$ and $\delta\rho_\gamma$). The blue (yellow) color of the iso-value contour stands for the positive (negative) sign of $\delta\rho$. The zoomed-in distribution of $\delta\rho$ in three dimensions around a single Fe, i.e. the orbital-order parameters Δ_{FO} and Δ_{HO} are displayed below. The inset shows the C_2 rotation axis and the xy -glide mirror plane that maintain unbroken.

affect the p-d hybridization but does not induce orbital order within the 3d-orbitals. The second term $-Tr\tilde{n}_j^2$ is a self-interaction correction, which can be most easily recognized if \tilde{n}_j is diagonal. In general, this term introduces new order parameters in the form of linear combinations of $\tilde{n}_j^{\alpha\beta}$. For example, the most-widely discussed ferro-orbital nematic order

$$\Delta_{FO} = \tilde{n}^{xz,xz} - \tilde{n}^{yz,yz} \quad (1)$$

is naturally covered by such a self-interaction correction term. When this negative quadratic term overturns the positive quadratic term coefficient of $E_{DFT}[\rho(\mathbf{r})]$ in a certain orbital-ordering channel, the corresponding symmetry breaking occurs.

After repeating the aforementioned numerical mini-

mization by using E_{DFT+U} with a typical $U = 3.6\text{eV}$ for iron-based superconductors, we identify additional local minima, and the symmetric $\rho(\mathbf{r})$ is no longer the global minimum. Fig. 1(b) shows the electron density contour at the symmetric local minimum [$\rho_\alpha(\mathbf{r})$]. The overall density distribution at the two new local minima [$\rho_{\beta/\gamma}(\mathbf{r})$] barely changes, because $\rho(\mathbf{r})$ contains contribution from all the valence electrons. In Figs. 1(c) and (d), we subtract $\rho_\alpha(\mathbf{r})$ from $\rho_{\beta/\gamma}(\mathbf{r})$. Now, the change of the density [$\delta\rho_{\beta/\gamma}(\mathbf{r})$] exhibits clear symmetry breaking patterns. The same type of symmetry breaking is reproduced by using the HSE06 hybrid functional [54, 55], which does not contain any material specific parameter (See below). We will also discuss the evolution of symmetry breaking as a function of U as well as other structural parameters later.

$\delta\rho_\beta(\mathbf{r})$ can be easily associated with the ferro-orbital nematic order Δ_{FO} . Indeed, the most noticeable change of \tilde{n}_j after the system reaches local minimum β is that $\tilde{n}^{xz,xz} - \tilde{n}^{yz,yz} \neq 0$. $\delta\rho_\gamma(\mathbf{r})$ in the form of high-rank multipoles is however unexpected. More surprisingly, while $\rho_\beta(\mathbf{r})$ gives an E_{DFT+U} very close to $\rho_\alpha(\mathbf{r})$, $\rho_\gamma(\mathbf{r})$ significantly reduces the total energy [Fig. 1(a)].

By inspecting \tilde{n}_j at local minimum γ , we notice the emergence of the off-diagonal terms $\tilde{n}^{yz,x^2-y^2} \approx \tilde{n}^{xz,xy} \neq 0$. We can define this orbital hybridization as a new order parameter:

$$\Delta_{HO} = (\tilde{n}^{yz,x^2-y^2} + \tilde{n}^{xz,xy})/2. \quad (2)$$

Without breaking the time-reversal symmetry, Δ_{HO} is real, which leads to a charge-density modulation around Fe atoms:

$$\begin{aligned} \delta\tilde{\rho}_{HO}(\mathbf{r}) &= \Delta_{HO}[\psi_{yz}(\mathbf{r})\psi_{x^2-y^2}(\mathbf{r}) + \psi_{xz}(\mathbf{r})\psi_{xy}(\mathbf{r})] \\ &\sim \Delta_{HO}R_{3d}^2(r)\sin^3\theta\cos\theta\sin3\phi \\ &\sim Y_4^{-3}(\theta, \phi) + Y_4^3(\theta, \phi), \end{aligned} \quad (3)$$

in which $R_{3d}(r)$ is the radial wavefunction of 3d-orbitals, (θ, ϕ) is the angular coordination of \mathbf{r} and Y_l^m is the spherical harmonic function. It is straightforward to check that $\delta\tilde{\rho}_{HO}$ indeed reproduces the basic features of $\delta\rho_\gamma$. Arising from the product of two $l = 2$ d-orbitals, it can be viewed as a g-wave orbital with the angular momentum $l = 4$. In addition, Fig. 1(d) shows that Δ_{HO} changes sign at the two Fe sites within a unit cell. Thus, our calculation suggests that an anti-ferro hexadecapolar order is favored in FeSe.

The emergence of Δ_{FO} or Δ_{HO} will generate novel reconstruction of the electronic structure. Let us first perform a simple group analysis. The factor group $(P4/nmm)/T$ is isomorphic to the point group D_{4h} , where T consists of all the lattice translation operators. A nonvanishing Δ_{FO} breaks D_{4h} down to the D_{2h} point group. A nonvanishing Δ_{HO} further breaks D_{2h} down to the C_{2v} point group. As indicated in the inset of Figs. 1(c) and (d), the remaining symmetry operators are: (1) a

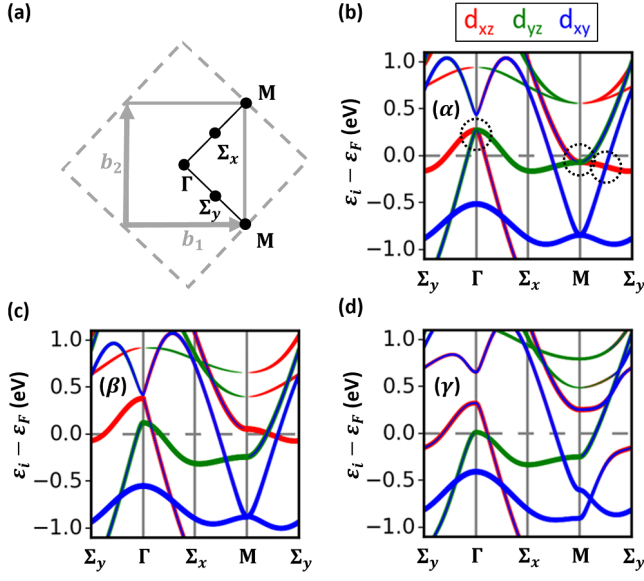


FIG. 2. (a) High-symmetry points used for the band calculation; b_1 and b_2 are the two reciprocal vectors of the 2-Fe Brillouin zone. The dashed square shows the 1-Fe Brillouin zone, for which $\Gamma - \Sigma_x(\Sigma_y) - M$ corresponds to the $X(Y)$ direction. (b)(c)(d) DFT+U band structures at local minima α , β , γ , respectively. The color of the bands denotes the orbital components. The dashed circles in (b) highlight the degenerate points that are split by Δ_{FO} and/or Δ_{HO} .

C_2 rotation along the x -axis; (b) a glide mirror reflection with respect to the xy -plane; and (3) the combination of the previous two, which can be viewed as a xz mirror passing the Se atoms.

In Fig. 2, we plot the DFT+U bands corresponding to $\rho_{\alpha, \beta, \gamma}$. The symmetric ρ_{α} produces the typical band structure of iron-based superconductors at the high-temperature tetragonal phase. Despite the widely-known overestimation of the band width and the pocket depth [5], the band degeneracy and orbital components around the Γ point (hole pocket) and the M point (electron pocket) can be compared with the ARPES data above the nematic transition temperature [24–27]. It is also well known that the degeneracy of d_{xz} and d_{yz} orbitals at these two points relies on the C_4 rotation. Breaking this symmetry thus leads to a splitting. Both ρ_{β} and ρ_{γ} correctly reproduce this feature.

A property that differentiates ρ_{γ} from ρ_{β} is whether the crossing of d_{xz} and d_{xy} bands along the $M - \Sigma_y$ direction as marked by the right dashed circle in Fig. 2(b) is gapped out. This crossing is protected by the C_2 rotation along the y -axis, under which the d_{xz} and d_{xy} orbitals have the opposite parity and thus do not hybridize [56]. This symmetry remains for ρ_{β} (D_{2h} group), but is broken for ρ_{γ} . Consequently, the $d_{xy}(d_{xz})$ -band that originally crosses the Fermi level between M and $\Sigma_y(\Sigma_x)$ is gapped out [Fig. 2(d)]. On the other hand, the crossing of the d_{yz} and d_{xy} bands along the $M - \Sigma_x$ direction is not af-

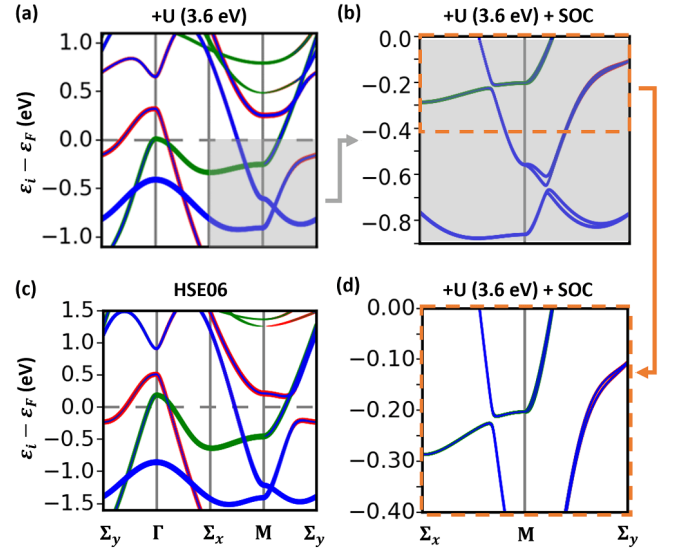


FIG. 3. (a) and (c) A comparison of the DFT+U and hybrid functional band structures at local minimum γ ; (b) and (d) Most noticeable band splitting when SOC is added. The color of the bands has the same denotation as in Fig. 2.

ected, because the C_2 rotation along the x -axis still exists in the C_{2v} point group. This in combination reduces the two electron pockets at the M point in the symmetric state [Fig. 2(b)] to one in the symmetry-broken state [Fig. 2(d)]. The missing of electron pocket in FeSe is long noticed in experiment, but controversies on the interpretation exist [25, 27–32, 37, 38, 57, 58]. This feature becomes more evident recently, thanks to the availability of fully detwinned single crystals [37, 38]. In addition, such orbital hybridization near the Fermi level causes a redistribution of electron population between the d_{xz} and d_{xy} orbitals, which was recently observed by nuclear magnetic resonance (NMR) at Fe sites [59]. In Figs. 3(a) and (c), we compare the DFT+U and hybrid functional band structures at local minima γ , it is clear that these important features associated with Δ_{HO} can also be obtained by hybrid functional calculation that does not contain any material specific parameter. We note that we have purposely adopted the same colors to denote the d_{xz} , d_{yz} and d_{xy} orbitals as commonly used in experiment, so a direct comparison can be made between our calculated bands and the experimental results, e.g. Fig. 4 in Ref. [37].

Besides, there is another feature uniquely associated with Δ_{HO} : while both D_{4h} and D_{2h} contain the inversion operator, it is lost in the C_{2v} point group. The original inversion center of FeSe is the mid point of two nearest-neighbor Fe. It is easy to examine that $\delta\rho_{\gamma}$ has a major component which is odd under such an inversion.

One immediate consequence of inversion symmetry breaking is that in general the double degeneracy of the bands (including the spin degree of freedom) will be re-

moved. To give a quantitative characterization, we include spin-orbit coupling (SOC) in E_{DFT+U} , and Figs. 3(b) and (d) highlight the regions, where the band splitting is most noticeable. Along the $M - \Sigma_x$ direction, double degeneracy is maintained, owing to the xz mirror symmetry. Nevertheless, the crossing of d_{yz} and d_{xy} bands, which is four-fold degenerate, gets split. The SOC gap size is of the order of 10 meV, much smaller than the Δ_{HO} -induced gap along the $M - \Sigma_y$ direction. Along the $M - \Sigma_y$ direction, SOC-induced splitting can be observed within the whole range, which might be resolved in high energy-resolution ARPES data. We notice that such type of splitting can already be observed in some existing ARPES data, e.g. Figs. 5(a) and (b) in the Supplementary Material of Ref. [34].

Another consequence of inversion symmetry breaking is the anisotropy of the electron spin. Noticing that the xy -plane is still a glide mirror in C_{2v} , the absence of inversion symmetry only generates electric field within the xy -plane. Coupling with the in-plane electron motion, the electron spin will be polarized along the z -direction. This is consistent with the recent neutron scattering measurement [16].

Moreover, the electronic inversion symmetry breaking couples to a special type of lattice distortion. According to the structural relaxation based on HSE06 functional, there is a small relative slide (0.002 Å) between Fe and Se layers along the (110) direction, i.e. the $C_2(x)$ axis as shown in Fig. 1. This type of lattice distortion was previously observed in $\text{LaFeAsO}_{1-x}\text{H}_x$ by X-ray diffraction (XRD) with a larger magnitude (0.13 Å) [60].

We note that the ARPES, neutron and XRD data mentioned above have alternative explanations. Therefore, the partial consistence between our results with the experiments cannot pin down the existence of an exotic parity-odd multipole orbital order. We propose that optical measurements sensitive to inversion symmetry breaking, e.g. second-harmonic generation [61, 62], can be applied to further test our scenario.

In the end, we summarize in Fig. 4 the evolution of symmetry breaking when we artificially tune the interaction strength (U), Fe-Fe distance ($a/\sqrt{2}$) and the out-of-plane coordination of Se (Z_{Se}). According to the energy evolution, as long as symmetry breaking occurs, our calculation indicates that the pure ferro-orbital ordering (E_β) in general has a higher energy than the multipolar one (E_γ). The multipolar ordering consists of a mixture of Δ_{HO} and Δ_{FO} , and typically Δ_{HO} has a larger amplitude. The multipole order vanishes when (1) the interaction strength becomes weak; (2) the lattice is compressive strained and (3) the buckling of the Se-Fe-Se sandwich is reduced.

We would like to thank Yan Zhang and Wei Li for helpful discussion. This work is supported by NSFC under Grant No. 11774196 and Tsinghua University Initiative Scientific Research Program. FW acknowledges support

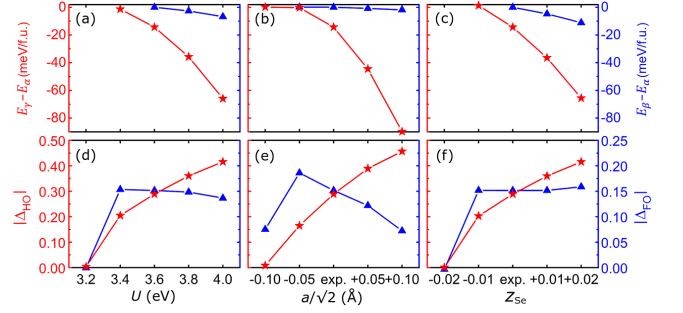


FIG. 4. The evolution of symmetry breaking as a function of the interaction strength (U), Fe-Fe distance ($a/\sqrt{2}$) and the out-of-plane coordinate of Se (Z_{Se}). (a-c) Energy evolution of local minima β (blue triangles) and γ (red stars) using the energy of local minimum α as the reference; (d-f) Amplitude of Δ_{HO} (red stars) and Δ_{FO} (blue triangles) at local minimum γ .

from the National Key Research and Development Program of China (Grand No. 2017YFA0302904).

* zheng-liu@tsinghua.edu.cn

- [1] N. L. Wang, H. Hosono, and P. Dai, *Iron-based superconductors: materials, properties and mechanisms* (CRC Press, 2012).
- [2] P. D. Johnson, G. Xu, and W.-G. Yin, *Iron-based superconductivity*, Vol. 211 (Springer, 2015).
- [3] P. Richard, T. Sato, K. Nakayama, T. Takahashi, and H. Ding, Reports on progress in physics **74**, 124512 (2011).
- [4] P. Dai, J. Hu, and E. Dagotto, Nature Physics **8**, 709 (2012).
- [5] Z. Yin, K. Haule, and G. Kotliar, Nature materials **10**, 932 (2011).
- [6] Z. Yin, K. Haule, and G. Kotliar, Nature physics **7**, 294 (2011).
- [7] R. M. Fernandes, A. V. Chubukov, and J. Schmalian, Nature physics **10**, 97 (2014).
- [8] A. Fedorov, A. Yaresko, T. Kim, Y. Kushnirenko, E. Haubold, T. Wolf, M. Hoesch, A. Grüneis, B. Büchner, and S. Borisenko, Scientific reports **6**, 36834 (2016).
- [9] J.-H. Chu, H.-H. Kuo, J. G. Analytis, and I. R. Fisher, Science **337**, 710 (2012).
- [10] C. Fang, H. Yao, W.-F. Tsai, J. Hu, and S. A. Kivelson, Physical Review B **77**, 224509 (2008).
- [11] C. Xu, M. Müller, and S. Sachdev, Physical Review B **78**, 020501 (2008).
- [12] R. Fernandes, A. Chubukov, J. Knolle, I. Eremin, and J. Schmalian, Physical Review B **85**, 024534 (2012).
- [13] C.-C. Lee, W.-G. Yin, W. Ku, et al., Physical Review Letters **103**, 267001 (2009).
- [14] C.-C. Chen, J. Maciejko, A. Sorini, B. Moritz, R. Singh, and T. Devereaux, Physical Review B **82**, 100504 (2010).
- [15] H. Kontani, T. Saito, and S. Onari, Physical Review B **84**, 024528 (2011).
- [16] M. Ma, P. Bourges, Y. Sidis, Y. Xu, S. Li, B. Hu, J. Li, F. Wang, and Y. Li, Physical Review X **7**, 021025 (2017).

- [17] V. I. Anisimov, F. Aryasetiawan, and A. Lichtenstein, *Journal of Physics: Condensed Matter* **9**, 767 (1997).
- [18] A. D. Becke, *The Journal of chemical physics* **98**, 1372 (1993).
- [19] J. Sun, K. Matsuura, G. Ye, Y. Mizukami, M. Shimozawa, K. Matsubayashi, M. Yamashita, T. Watashige, S. Kasahara, Y. Matsuda, J. Q. Yan, B. C. Sales, Y. Uwatoko, J. G. Cheng, and T. Shibauchi, *Nature communications* **7**, 12146 (2016).
- [20] Q. Wang, Y. Shen, B. Pan, X. Zhang, K. Ikeuchi, K. Iida, A. Christianson, H. Walker, D. Adroja, M. Abdel-Hafiez, X. Chen, D. A. Chareev, A. N. Vasiliev, and J. Zhao, *Nature communications* **7**, 12182 (2016).
- [21] W. Qing-Yan, L. Zhi, Z. Wen-Hao, Z. Zuo-Cheng, Z. Jin-Song, L. Wei, D. Hao, O. Yun-Bo, D. Peng, C. Kai, J. Wen, C.-L. Song, K. He, J.-F. Jia, S.-H. Ji, Y.-Y. Wang, L.-L. Wang, X. Chen, X.-C. Ma, and Q.-K. Xue, *Chinese Physics Letters* **29**, 037402 (2012).
- [22] J.-F. Ge, Z.-L. Liu, C. Liu, C.-L. Gao, D. Qian, Q.-K. Xue, Y. Liu, and J.-F. Jia, *Nature materials* **14**, 285 (2015).
- [23] K. Nakayama, Y. Miyata, G. Phan, T. Sato, Y. Tanabe, T. Urata, K. Tanigaki, and T. Takahashi, *Physical review letters* **113**, 237001 (2014).
- [24] T. Shimojima, Y. Suzuki, T. Sonobe, A. Nakamura, M. Sakano, J. Omachi, K. Yoshioka, M. Kuwata-Gonokami, K. Ono, H. Kumigashira, A. E. Böhrer, F. Hardy, T. Wolf, C. Meingast, H. v. Löhneysen, H. Ikeda, and K. Ishizaka, *Physical Review B* **90**, 121111 (2014).
- [25] Y. Suzuki, T. Shimojima, T. Sonobe, A. Nakamura, M. Sakano, H. Tsuji, J. Omachi, K. Yoshioka, M. Kuwata-Gonokami, T. Watashige, R. Kobayashi, S. Kasahara, T. Shibauchi, Y. Matsuda, Y. Yamakawa, H. Kontani, and K. Ishizaka, *Physical Review B* **92**, 205117 (2015).
- [26] P. Zhang, T. Qian, P. Richard, X. Wang, H. Miao, B. Lv, B. Fu, T. Wolf, C. Meingast, X. Wu, Z. Q. Wang, J. P. Hu, and H. Ding, *Physical Review B* **91**, 214503 (2015).
- [27] M. Watson, T. Kim, A. Haghighirad, N. Davies, A. McCollam, A. Narayanan, S. Blake, Y. Chen, S. Ghanadzadeh, A. Schofield, M. Hoesch, C. Meingast, T. Wolf, and A. I. Coldea, *Physical Review B* **91**, 155106 (2015).
- [28] M. Watson, T. Kim, L. Rhodes, M. Eschrig, M. Hoesch, A. Haghighirad, and A. Coldea, *Physical Review B* **94**, 201107 (2016).
- [29] M. D. Watson, A. A. Haghighirad, L. C. Rhodes, M. Hoesch, and T. K. Kim, *New Journal of Physics* **19**, 103021 (2017).
- [30] L. C. Rhodes, M. D. Watson, A. A. Haghighirad, D. V. Evtushinsky, M. Eschrig, and T. K. Kim, *Physical Review B* **98**, 180503 (2018).
- [31] H. Xu, X. Niu, D. Xu, J. Jiang, Q. Yao, Q. Chen, Q. Song, M. Abdel-Hafiez, D. Chareev, A. Vasiliev, Q. S. Wang, H. L. Wo, J. Zhao, R. Peng, and D. L. Feng, *Physical review letters* **117**, 157003 (2016).
- [32] Y. Zhang, M. Yi, Z.-K. Liu, W. Li, J. Lee, R. Moore, M. Hashimoto, M. Nakajima, H. Eisaki, S.-K. Mo, Z. Hussain, T. P. Devereaux, Z.-X. Shen, and D. H. Lu, *Physical Review B* **94**, 115153 (2016).
- [33] L. Fanfarillo, J. Mansart, P. Toulemonde, H. Cercellier, P. Le Fèvre, F. Bertran, B. Valenzuela, L. Benfatto, and V. Brouet, *Physical Review B* **94**, 155138 (2016).
- [34] Y. Kushnirenko, A. Fedorov, E. Haubold, S. Thirupathaiiah, T. Wolf, S. Aswartham, I. Morozov, T. Kim, B. Büchner, and S. Borisenko, *Physical Review B* **97**, 180501 (2018).
- [35] D. Liu, C. Li, J. Huang, B. Lei, L. Wang, X. Wu, B. Shen, Q. Gao, Y. Zhang, X. Liu, Y. Hu, Y. Xu, A. Liang, J. Liu, P. Ai, L. Zhao, S. He, L. Yu, G. Liu, Y. Mao, X. Dong, X. Jia, F. Zhang, S. Zhang, F. Yang, Z. Wang, Q. Peng, Y. Shi, J. Hu, T. Xiang, X. Chen, Z. Xu, C. Chen, and X. J. Zhou, *Physical Review X* **8**, 031033 (2018).
- [36] Z. Wang, H. Zhang, D. Liu, C. Liu, C. Tang, C. Song, Y. Zhong, J. Peng, F. Li, C. Nie, L. Wang, X. J. Zhou, X. Ma, Q. K. Xue, and F. Liu, *Nature materials* **15**, 968 (2016).
- [37] M. Yi, Y. Zhang, H. Pfau, T. Chen, Z. Ye, M. Hashimoto, R. Yu, Q. Si, D.-H. Lee, P. Dai, Z.-X. Shen, D. Lu, and R. J. Birgeneau, *arXiv preprint arXiv:1903.04557* (2019).
- [38] S. Huh, J. Seo, B. Kim, S. Cho, J. Jung, S. Kim, Y. Koh, C. Kwon, J. Kim, W. Kyung, J. D. Denlinger, Y. Kim, B. Chae, N. Kim, Y. Kim, and C. Kim, *arXiv preprint arXiv:1903.08360* (2019).
- [39] Y. Su, H. Liao, and T. Li, *Journal of Physics: Condensed Matter* **27**, 105702 (2015).
- [40] S. Onari, Y. Yamakawa, and H. Kontani, *Physical review letters* **116**, 227001 (2016).
- [41] R.-Q. Xing, L. Classen, and A. V. Chubukov, *Physical Review B* **98**, 041108 (2018).
- [42] M. Cococcioni and S. De Gironcoli, *Physical Review B* **71**, 035105 (2005).
- [43] R. M. Martin, *Electronic structure: basic theory and practical methods* (Cambridge university press, 2004).
- [44] G. Kresse and J. Furthmüller, *Physical review B* **54**, 11169 (1996).
- [45] M. C. Payne, M. P. Teter, D. C. Allan, T. Arias, and A. J. Joannopoulos, *Reviews of modern physics* **64**, 1045 (1992).
- [46] F. Wang, S. A. Kivelson, and D.-H. Lee, *Nature Physics* **11**, 959 (2015).
- [47] J. Glasbrenner, I. Mazin, H. O. Jeschke, P. Hirschfeld, R. Fernandes, and R. Valentí, *Nature Physics* **11**, 953 (2015).
- [48] K. Liu, Z.-Y. Lu, and T. Xiang, *Physical Review B* **93**, 205154 (2016).
- [49] F. Zheng, Z. Wang, W. Kang, and P. Zhang, *Scientific reports* **3**, 2213 (2013).
- [50] T. Shishidou, D. F. Agterberg, and M. Weinert, *Communications Physics* **1**, 8 (2018).
- [51] T. M. McQueen, Q. Huang, V. Ksenofontov, C. Felser, Q. Xu, H. Zandbergen, Y. S. Hor, J. Allred, A. J. Williams, D. Qu, J. Checkelsky, N. P. Ong, and R. J. Cava, *Physical Review B* **79**, 014522 (2009).
- [52] J. P. Perdew, K. Burke, and M. Ernzerhof, *Physical review letters* **77**, 3865 (1996).
- [53] S. Dudarev, G. Botton, S. Savrasov, C. Humphreys, and A. Sutton, *Physical Review B* **57**, 1505 (1998).
- [54] J. Heyd, G. E. Scuseria, and M. Ernzerhof, *The Journal of chemical physics* **118**, 8207 (2003).
- [55] J. Heyd, G. E. Scuseria, and M. Ernzerhof, *The Journal of chemical physics* **124**, 219906 (2006).
- [56] V. Cvetkovic and O. Vafek, *Physical Review B* **88**, 134510 (2013).
- [57] P. O. Sprau, A. Kostin, A. Kreisel, A. E. Böhrer, V. Taufour, P. C. Canfield, S. Mukherjee, P. J. Hirschfeld, B. M. Andersen, and J. S. Davis, *Science* **357**, 75 (2017).
- [58] A. Kostin, P. O. Sprau, A. Kreisel, Y. X. Chong, A. E.

- Böhmer, P. C. Canfield, P. J. Hirschfeld, B. M. Andersen, and J. S. Davis, *Nature materials* , 1 (2018).
- [59] J. Li, B. Lei, D. Zhao, L. Nie, D. Song, L. Zheng, S. Li, B. Kang, X. Luo, T. Wu, and X. H. Chen, arXiv preprint arXiv:1903.05798 (2019).
- [60] M. Hiraishi, S. Iimura, K. M. Kojima, J.-i. Yamaura, H. Hiraka, K. Ikeda, P. Miao, Y. Ishikawa, S. Torii, M. Miyazaki, *et al.*, *Nature physics* **10**, 300 (2014).
- [61] L. Zhao, C. Belvin, R. Liang, D. Bonn, W. Hardy, N. Armitage, and D. Hsieh, *Nature Physics* **13**, 250 (2017).
- [62] J. Harter, H. Chu, S. Jiang, N. Ni, and D. Hsieh, *Physical Review B* **93**, 104506 (2016).